Scilight

*Membrane Technologies Research*
https://www.sciltp.com/journals/mtr

*Article*

# Effect of Microstructure in MOR Membrane on its Adsorption and Permeation Properties for Water and Acetic Acid

Motomu Sakai [1,*], Yuhei Imanishi [1], Masatoshi Narashima [1], Masahiro Seshimo [1] and Masahiko Matsukata [1,2,3]

[1] Department of Applied Chemistry, Waseda University, 513 Wasedatsurumaki-cho, Shinjuku-ku, Tokyo 162-0041, Japan
[2] Research Organization for Nano & Life Innovation, Waseda University, 513 Wasedatsurumaki-cho, Shinjuku-ku, Tokyo 162-0041, Japan
[3] Advanced Research Institute for Science and Engineering, Waseda University, 513 Wasedatsurumaki-cho, Shinjuku-ku, Tokyo 162-0041, Japan
* Correspondence: saka.moto@aoni.waseda.jp

**How To Cite:** Sakai, M.; Imanishi, Y.; Narashima, M.; et al. Effect of Microstructure in MOR Membrane on its Adsorption and Permeation Properties for Water and Acetic Acid. *Membrane Technologies Research* **2025**, *1*(1), 1.

Received: 31 December 2024
Revised: 20 July 2025
Accepted: 3 September 2025
Published: 19 September 2025

**Abstract:** The effect of crystal orientation on the permeation and separation performance of MOR-type membrane for water/acetic acid mixtures was investigated. The crystal orientation of MOR membrane was controlled by changing the water content of the synthesis gel. The orientation gradually changed from *c*-orientation to random orientation with increasing water content. Regardless of their crystal orientation, both membranes exhibited the extremely high separation performances (a > 10,000). *c*-Oriented MOR membrane showed a higher water flux than that through randomly oriented membrane in the unary systems. In contrast, the water flux through *c*-oriented membrane decreased in the binary system, because acetic acid molecules in the 12-ring along the *c*-axis hindered water permeation. The randomly oriented membrane maintained a relatively high water flux even in the binary system possibly because the 8-ring along *b*-axis avoided the entering of acetic acid. From the results of the adsorption test of acetic acid on MOR powder and randomly oriented membrane, the adsorbed amount on the membrane was approximately 30% less than that on MOR powder, suggesting that acetic acid can only access the part of crystals in a membrane layer. The region inside the membrane, where acetic acid cannot enter, contributes to its extremely high separation performance.

**Keywords:** zeolite; membrane; microstructure; adsorption; water; acetic acid

## 1. Introduction

Dehydration from water/acetic acid mixture has often been required in several processes that produce acetic acid derivatives or use acetic acid as a solvent. Currently, a water/acetic acid mixture is distilled with a large reflux ratio to recover acetic acid with a purity of >97 wt%. Separation of water from acetic acid by distillation consumes a large amount of energy due to the low relative volatility and large evaporative latent heat of water. Membrane separation has attracted considerable attention as a novel energy-saving method for acetic acid dehydration.

The hybrid process of membrane separation and distillation process has attracted attention as a promising energy-saving technology [1–3]. For the dehydration of a water/acetic acid vapor mixture, high heat, and acid resistance are required for the membrane material used in the membrane separation/distillation hybrid system. Therefore, inorganic membranes have been studied for the separation of water/acetic acid mixtures.

Zeolite membranes offer considerable potential because their chemical and physical properties can be controlled by their topology and Si/Al ratio. Previously, some zeolite membranes have been used for the separation of water/acetic acid mixture [4–10]. In particular, MOR-type zeolite has been expected as one of the most promising materials due to its superior separation performance and acid resistance [8–10]. Sato et al. reported MOR-type membrane with a water flux of 10.9 kg $m^{-2}$ $h^{-1}$ and separation factor of ca. 500 for a water/acetic acid mixture (50/50 wt%) at 403 K [8]. In previous studies [10,11], we developed a synthesis method for a defect-free MOR membrane and reported its separation properties for water/acetic acid mixtures. Although a number of MOR membranes with excellent separation performance have been reported in practice, the separation mechanism of water and acetic acid has not been fully elucidated.

For zeolites with anisotropic pore networks, the orientation of the crystal in a membrane often influences its permeation and separation properties [12–15]. The effect of crystal orientation in membranes on their permselectivities is one of the hottest topics in the field of polycrystalline membranes [16–19]. MOR has an anisotropic pore network, e.g., a 12-ring (0.70 × 0.65 nm) and an 8-ring (0.57 × 0.26 nm) along the *c*-axis, and an 8-ring (0.34 × 0.48 nm) along the *b*-axis [20,21], as shown in Figure 1. Water, which has the molecular size of 0.28 nm, can enter both the 12- and 8-rings. In contrast, acetic acid can enter the 12-ring and not the 8-ring due to its bulky size of 0.44 nm [22]. When 12-ring penetrates through a membrane, acetic acid can permeate through the membrane, resulting in the deterioration of the separation performance. Therefore, crystal orientation plays an important role in the separation. In particular, to effectively utilize the molecular sieving effect based on the 8-ring, the crystal orientation needs to be precisely controlled.

In addition to crystal orientation, the microstructure at grain boundaries also has a major influence on the performance of zeolite membranes [23–25]. For example, a number of grain boundaries form by the collision of two crystals inside a membrane, resulting in narrowing and sometimes obstruction of micropores due to the mismatch of crystal faces. Previously, we reported that the apparent pore size in MFI-type zeolite membrane narrowed at the grain boundaries to 0.49 nm from the original pore size of 0.55 nm [23]. In the case of MOR membrane, such microstructure inside a membrane may contribute to the separation performance as well. Previously, the orientation of MOR membrane was controlled by changing the composition of synthesis gel [11]. MOR membrane prepared by concentrated and diluted gel exhibited *c*-orientation and *a,b*-orientation.

In this study, we shed light on the contribution of crystal orientation and microstructure to the performance of MOR membranes. The crystal orientations of the MOR membranes were controlled by varying synthesis conditions. The effect of crystal orientation on the permeation and separation properties of a water/acetic acid mixture was studied. In addition, the principle of separation of water and acetic acid was considered based on adsorption tests for the MOR powder crystal and membrane.

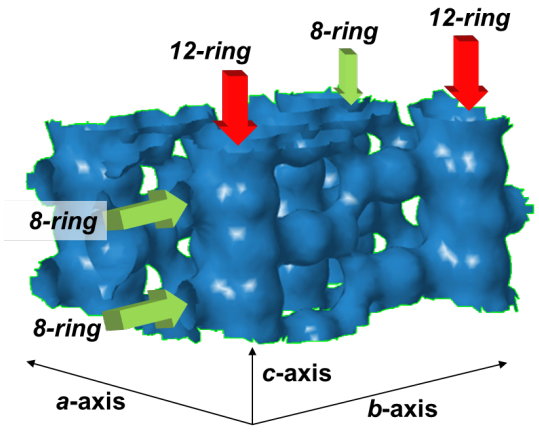


**Figure 1.** Pore-network of MOF-type zeolite.

## 2. Experimental

### *2.1. Procedure of Membrane Preparation*

MOR membrane was prepared by seed-assisted synthesis on the outer surface of a porous tubular a-alumina support (inner diameter = 7 mm, outer diameter = 10 mm) [10,11]. The effective membrane area was 6.28 $cm^2$.

A given amount of MOR powder (HSZ 600HOA; $SiO_2/Al_2O_3$ = 10.2, Tosoh Co., Tokyo, Japan) was ground using an agate mortar. The ground MOR crystals were dispersed in distilled water at a solid concentration of 1.8

g $L^{-1}$. Seed crystals were loaded onto the outer surface of the support by dip-coating with a MOR colloidal suspension. A tubular support, both ends of which were plugged with polytetrafluoroethylene (PTFE) caps, was immersed in the suspension for 1 min. The support was then withdrawn vertically from the suspension and dried for 2 h at 343 K. The seeding procedure was performed twice.

The seeded support was placed vertically in a PTFE-lined stainless steel autoclave with a synthesis gel. Four types of MOR membranes were prepared using synthesis gels with a molar composition of $10Na_2O$: $0.15Al_2O_3$: $36SiO_2$: $xH_2O$ ($x$ = 460, 627, 960, and 1127). We named the membranes $MOR_{460}$, $MOR_{627}$, $MOR_{960}$, and $MOR_{1127}$, respectively. The synthesis mixtures were prepared by mixing colloidal silica (ST-S; Nissan Chemical Ind. Ltd., Tokyo, Japan), sodium aluminate ($Na_2O$, 33 wt%, $Al_2O_3$ 37 wt%, Kanto Chemical Co. Inc., Tokyo, Japan), sodium hydroxide (>97 wt%, Kanto Chemical Co. Inc.), and distilled water. The colloidal silica was slowly added to a solution of sodium aluminate and sodium hydroxide. Each synthesis mixture was aged at 323 K for 4 h prior to crystallization. The autoclave was then placed in a preheated oven for hydrothermal crystallization at 453 K for 6 h. After crystallization, the autoclave was quenched with tap water. The as-synthesized samples were then rinsed with distilled water until the pH of the wash solution was neutral. The membrane was then washed in boiling water for 12 h and dried at 383 K for 12 h. The amount of zeolite formed on the support was defined as the difference in weight between the bare support and the membrane after drying.

### *2.2. Characterizations of Synthesized Membrane*

The phase and orientation of the zeolite layer formed on the support surface was evaluated by X-ray diffraction (XRD, Rigaku Ultima IV) using Cu Kα radiation at 40 kV and 20 mA with a scan speed of 2 deg (2$q$) $min^{-1}$. The intensities of the (150) and (002) planes at 22.2° and 23.6° were used to evaluate the orientation of the crystal layer.

The membrane thickness and the morphological features of the membrane surface were observed by field-emission scanning electron microscopy (FE-SEM; Hitachi S-4800, Hitachi High-Tech Co., Tokyo, Japan). The Si/Al ratio of the zeolite layer was analyzed by energy-dispersive X-ray spectroscopy.

### *2.3. Vapor Permeation Test*

The permeation and separation properties of MOR membranes for water and acetic acid were studied in the vapor permeation mode. The tubular membrane was fixed inside a membrane module using graphite O-rings. Water and acetic acid vapors were fed to the outer surface of the membrane at a given partial pressure balanced by the helium diluent gas. The permeate side was swept with flowing helium. The feed and permeate sides were maintained at atmospheric pressure. The permeate was analyzed for its composition using a gas chromatograph equipped with a thermal conductivity detector (GC-TCD; Shimadzu GC-14B, Shimadzu Co., Kyoto, Japan). The separation factor, a (−), was defined by Equation (1),

$$\mathrm{a} = (Y_\mathrm{W}\ Y_\mathrm{A}^{-1})/(X_\mathrm{W}\ X_\mathrm{A}^{-1})^{-1} \quad (1)$$

where $Y_\mathrm{W}$ and $Y_\mathrm{A}$ represent the partial pressures of water and acetic acid in the permeate, respectively. $X_\mathrm{W}$ and $X_\mathrm{A}$ represent those in the feed, respectively. The flux $J$ (mol $m^{-2}$ $s^{-1}$) was calculated using Equation (2):

$$J = u\ A^{-1} \quad (2)$$

where $u$ is the permeate flow rate (mol $s^{-1}$), and $A$ is the effective membrane area ($m^2$).

### *2.4. Adsorption Measurement*

The adsorption properties of water and acetic acid on MOR powder crystals and membrane were evaluated by a gravimetric method using a home-made apparatus, as shown in Figure 2.

The measurement procedure was as follows. Water and/or acetic acid vapors were fed into the MOR powder or membrane placed in a sample holder. The temperature of the sample holder was controlled by using a heating jacket. The partial pressure of the vapor was adjusted using helium as a diluent gas. The temperature and partial pressure were varied in the ranges 398–473 K and 1–50 kPa, respectively. The vapor was fed into the sample for a sufficient period until the adsorbed amount reached a plateau, more than 3 h. Then, the vapor supply was stopped, and the sample holder was purged with helium for a short period. Finally, the adsorbed molecules were desorbed under vacuum and collected in cold traps using liquid nitrogen. The weight of the trapped liquid was analyzed for its composition by GC-TCD to calculate the amounts of adsorbed water and acetic acid.

1.00 g of dried MOR powder (HSZ 600HOA; $SiO_2/Al_2O_3$ = 10.2, Tosoh Co., Tokyo, Japan) was used as a sample. For the measurement using membrane, the entire membrane was placed in a sample holder without

breaking it. The weights of zeolite membrane prepared on alumina supports were determined as follows. The weight of a dried support was measured before membrane preparation, and the weight of a dried support + membrane was re-measured after membrane preparation. The difference in these weight means the weight of zeolite synthesized on the support. Six tubular membranes synthesized under the same conditions were placed in the sample tube, as shown in Figure 2. The sample was preheated at 573 K for 3 h in an argon stream to remove adsorbed water and gases prior to measurements.

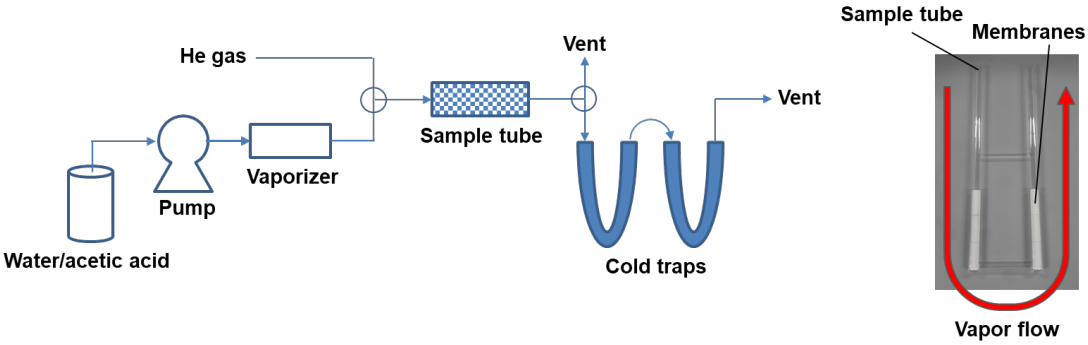


**Figure 2.** Schematic diagram of the apparatus for adsorption measurement and photograph of sample tube.

## 3. Results

### *3.1. Effect of Water Content in Synthesis Gel on Crystal Orientation*

The orientations of the crystals in MOR membranes grown in the different synthesis gels were evaluated by microscopic observation and XRD. Figure 3 shows the typical FE-SEM images of MOR membranes. The FE-SEM images revealed that the support surface was fully covered with numerous small MOR crystals in all cases. The thicknesses and Si/Al ratios of the crystal layer in each MOR membrane were almost the same, i.e., ca. 3 μm and 5, respectively.

The morphological features of the membrane surface were strongly influenced by the water content of the synthesis gel. In the membranes synthesized with lower water contents ($MOR_{460}$ and $MOR_{627}$), hexagonal faces were observed on the outer surface. In contrast, a hexagonal face was rarely observed on the surface of the membranes synthesized with higher water contents ($MOR_{960}$, $MOR_{1127}$).

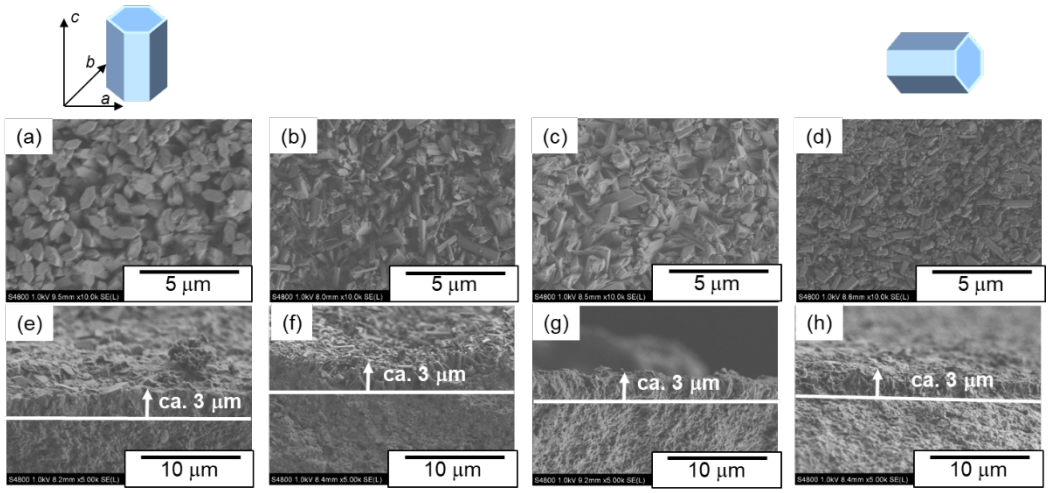


**Figure 3.** Typical FE-SEM images of MOR membranes. The upper and lower figures show the membrane surface and cross-section, respectively. (**a**,**e**) $MOR_{460}$; (**b**,**f**) $MOR_{627}$; (**c**,**g**) $MOR_{960}$; (**d**,**h**) $MOR_{1127}$.

Figure 4 shows the XRD patterns of the membranes and the intensities of the (150) and (002) reflection peaks, which are an index of membrane orientation. All the diffraction patterns of the membranes were identical to that of a typical MOR crystal, indicating that the crystal layers formed on the support had a pure MOR phase. For the membranes synthesized with a lower water content mixture, the intensities of the (002) peaks were comparatively strong, indicating that the crystals were oriented with the (002) face parallel to the support surface. In contrast, the

intensity of the (150) peak increased with increasing water content. The ratio of (002) to (150) decreased from 0.391 to 0.160, indicating that the crystal layer grown in the diluted synthesis gel was randomly oriented.

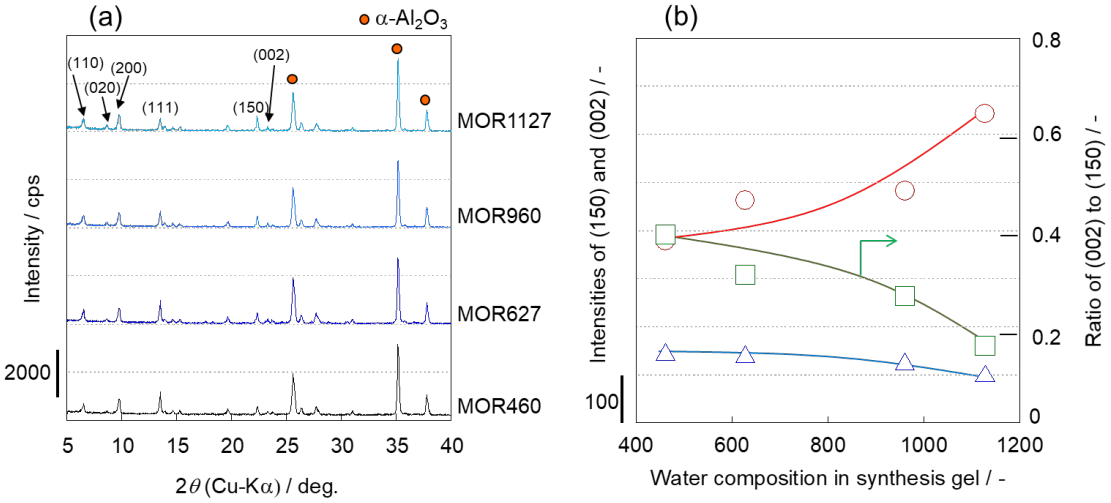


**Figure 4.** (**a**) XRD patterns of MOR membranes. (**b**) Intensities of diffraction peaks ○ (150) and △ (002). □ the ratio of (002) to (150).

### *3.2. Permeation and Separation Properties of MOR Membranes*

Permeation tests were conducted for the prepared MOR membranes. Water vapor was fed to the membranes in the unary systems at 10 kPa using a dilution gas. For the binary separation tests, the partial pressures of water and acetic acid were adjusted to 10 kPa. All permeation tests were carried out at 398 K. Figure 5 shows the fluxes and relative fluxes of water through the MOR membranes with different orientations. We define the relative flux, $J_R$, as the flux in a binary system, $J_B$, divided by that in a unary system, $J_U$, according to Equation (3).

$$J_R = J_B J_U^{-1} \tag{3}$$

In unary systems, the membranes synthesized with a lower water content showed higher water fluxes. The water fluxes through $MOR_{460}$ and $MOR_{1127}$ were 21 and 16 mmol $m^{-2}$ $s^{-1}$, respectively. In binary systems, the water flux was reduced by the presence of acetic acid. For example, the water fluxes through $MOR_{460}$ and $MOR_{1127}$ were 4.3 and 8.6 mmol $m^{-2}$ $s^{-1}$, respectively. Membranes prepared in the diluted synthesis gel showed a higher water flux in the binary system, with a change in the relative water flux from 0.25 to 0.49.

Note that the acetic acid fluxes were below the detection limit ($1.0 \times 10^{-7}$ mol $m^{-2}$ $s^{-1}$) in all binary systems. Therefore, these MOR membranes exhibited extremely high separation properties (a > 10,000). In other words, the purities of water penetrating through MOR membranes were > 99.95 wt%.

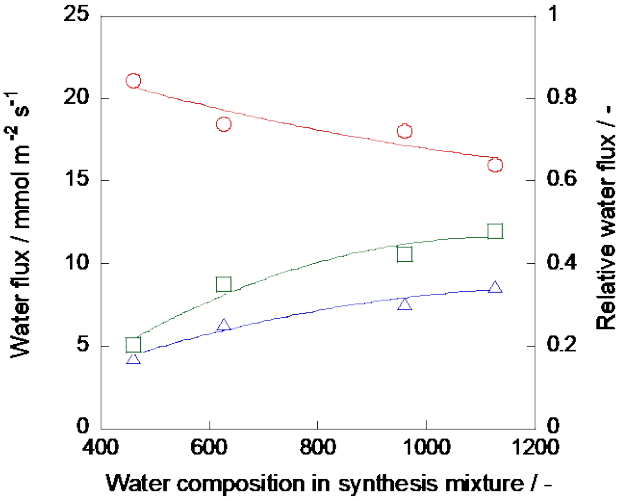


**Figure 5.** Water flux through MOR membranes. ○, water flux in unary system; △, water flux in binary system; □, relative water flux.

### *3.3. Temperature Dependency of Permeation Property of Randomly Oriented MOR Membrane*

More detailed permeation and separation properties were studied for $MOR_{1127}$, which, as described above, exhibited a relatively high water flux for the water/acetic acid binary mixture. Figure 6 shows the temperature dependence of the water fluxes through $MOR_{1127}$ in the unary and binary systems. In the unary system, the partial pressure of water was controlled at 10, 25, and 50 kPa using helium dilution gas. For the binary systems, an equimolar mixture of water and acetic acid was fed to the membrane. The partial pressure of the vapor mixture was controlled at 20, 50, and 100 kPa using a dilution gas.

In unary systems, the water fluxes increased with increasing membrane temperature at higher partial pressures of 25 and 50 kPa. Only at the lowest partial pressure of 10 kPa, the water flux slightly decreased with increasing temperature. The water fluxes in the binary systems were lower than those in the unary systems due to the inhibition of acetic acid, as well as the result shown in Figure 4b. The water fluxes in the binary systems increased with increasing temperature and approached those in the unary systems. As shown in Figure 5, acetic acid fluxes were below the detection limit ($1.0 \times 10^{-7}$ mol $m^{-2}$ $s^{-1}$) in all the binary systems.

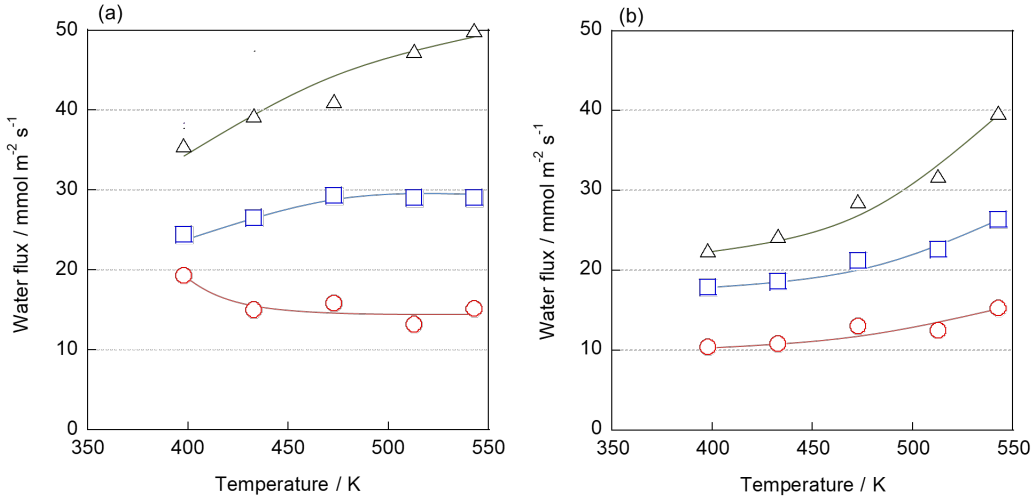


**Figure 6.** Temperature dependencies of water fluxes through $MOR_{1127}$ in (**a**) unary and (**b**) binary systems. In the binary system, an equimolar mixture of water and acetic acid was used. ○ 10, □ 25, and △ 50 kPa of water vapor in unary systems; ○ 10/10, □ 25/25, and △ 50/50 kPa of water/acetic acid vapor in binary systems.

### *3.4. Adsorption Property of Water and Acetic Acid on MOR Powder Crystal*

The amounts of water and acetic acid adsorbed on MOR zeolite in the unary and binary systems were measured, and the effect of competitive adsorption on the adsorbed amounts was studied.

Figure 7 shows the adsorption isotherms of water and acetic acid on MOR crystal powder. The adsorbed amounts of water in the unary systems increased with increasing partial pressure of water and were almost saturated above 30 kPa. The saturated amounts of water were 14.8 and 4.90 molecules per unit cell at 398 and 543 K, respectively, at 50 kPa. In the binary systems, the adsorbed amounts of water were relatively smaller than those of the unary systems, e.g., 11.5 and 4.41 molecules per unit cell at 398 and 543 K, respectively.

The amount of acetic acid adsorbed was generally smaller than that of water. For example, 2.76 and 0.85 molecules were adsorbed per unit cell at 398 and 543 K, respectively, at 50 kPa in the unary systems. In the binary systems, these amounts decreased to 2.42 and 0.37, suggesting that water and acetic acid were competitively adsorbed on MOR zeolite.

Figure 8 shows the isotherms for the $MOR_{1127}$ membrane in the unary and binary systems. The adsorbed amounts and behavior of water were almost the same as those on the crystal powder, e.g., 15.1 and 5.03 molecules per unit cell at 398 and 543 K, respectively, at 50 kPa. In contrast, the amount of acetic acid adsorbed on the membrane was smaller than that on the powder crystal in both the unary and binary systems. For example, the amount adsorbed onto the membrane was approximately 30% smaller than on the powder at 398 K and 50 kPa.

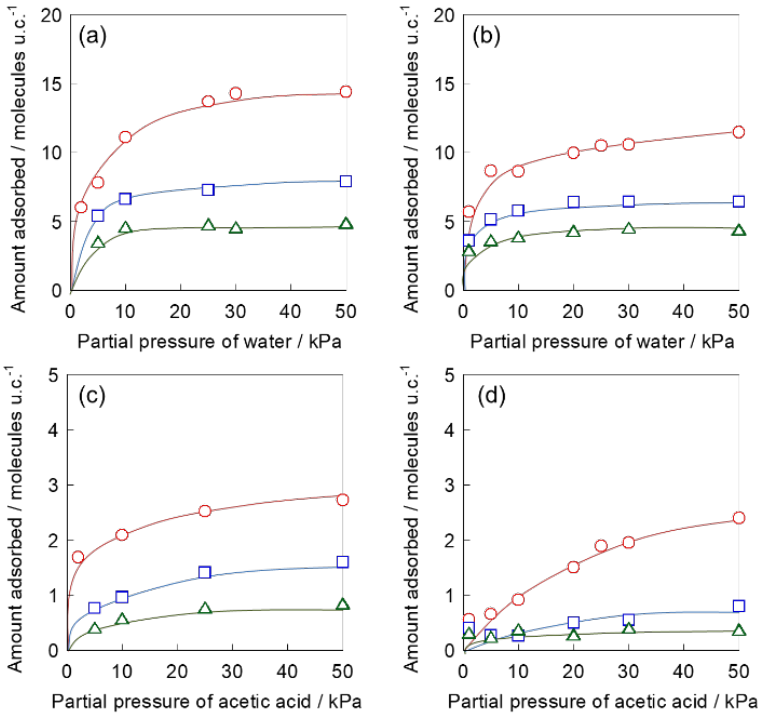


**Figure 7.** Adsorption isotherms of water and acetic acid on MOR powdery crystal. In the binary system, an equimolar mixture of water and acetic acid was fed. (**a**) water in unary system; (**b**) water in binary system; (**c**) acetic acid in unary system; (**d**) acetic acid in binary system. ○ 398, □ 473, △ 543 K.

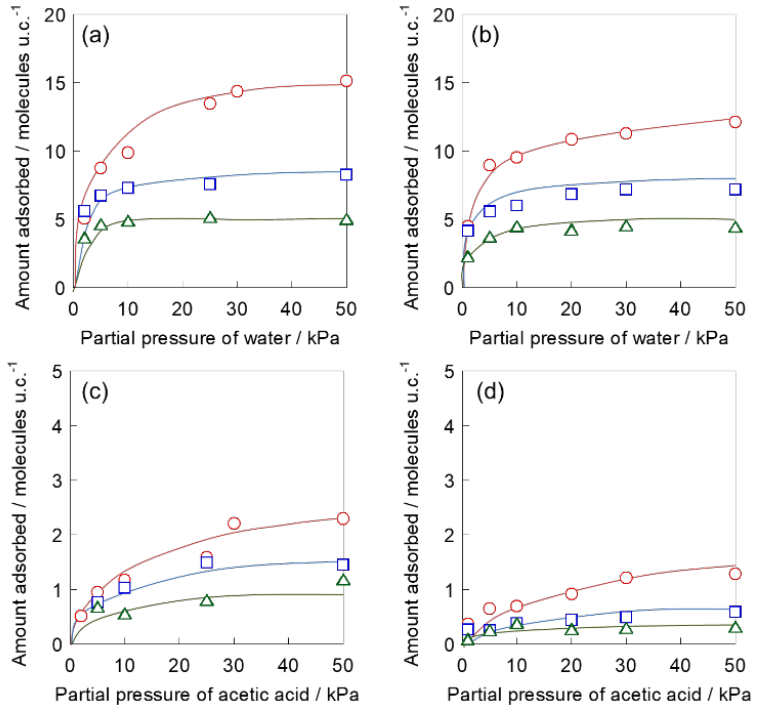


**Figure 8.** Adsorption isotherms of water and acetic acid on $MOR_{1127}$ membrane. In the binary system, an equimolar mixture of water and acetic acid was fed. (**a**) water in unary system; (**b**) water in binary system; (**c**) acetic acid in unary system; (**d**) acetic acid in binary system. ○ 398, □ 473, △ 543 K.

## 4. Discussion

### *4.1. Crystal Orientation and Microstructure in MOR Membrane*

Typical MOR crystals exhibit a hexagonal columnar shape, in which the *a,b*-plane forms a hexagonal face [26]. Therefore, the orientation of the crystal layer on the membrane surface can be estimated from microscopic

observations. Consequently, a *c*-oriented membrane was prepared in a synthesis gel with a low water content, $MOR_{460}$. The *a,b*-plane, in which a large pore exists, was exposed on the surface of the membrane. In contrast, fewer hexagonal planes can be observed on the surface of a randomly oriented membrane prepared by a diluted synthesis gel of $MOR_{1127}$. In the randomly oriented membrane, small pores were also exposed along the *b*-axis. This change in orientation, judged by the FE-SEM observations, is consistent with the XRD results.

In a previous study [11], Li et al. reported the effect of water content on the growth of MOR membranes. They explained that the *c*-oriented MOR membrane was obtained by the "evolutionary selection" mechanism. In this mechanism, many crystals lie under the surface layer, and only those crystals in which the fastest growth direction were perpendicular to the support surface, survive. Since MOR crystals grew the fastest along the *c*-axis, a *c*-oriented layer was observed on the top surface of the membrane. Notably, a layer of crystals with no particular orientation exists inside membrane, although evolutionary selection determines the orientation near the surface.

The membrane synthesized with a mixture with higher water content did not show the *c*-orientation. A large number of small crystals were observed in the FE-SEM images, indicating that randomly oriented membranes formed by repeated heterogeneous nucleation. Although nucleation occurs frequently, evolutionary selection based on crystal growth may not progress. We believe that this is the reason for the random orientation of the membrane.

As a result, the orientations of the surface crystal layer of MOR membrane were successfully manipulated by changing the water content in the synthesis gel.

### *4.2. Effect of Membrane Orientation on Water Permeation*

Here, we discuss why acetic acid could not permeate through MOR membranes. The kinetic diameters of water and acetic acid are 0.28 and 0.44 nm, respectively [22]. As described in the introduction, acetic acid could enter the 12-ring, 0.70 × 0.65 nm along the *c*-axis, but not the 8-rings, 0.34 × 0.48 nm and 0.26 × 0.57 nm along the *b*- and *c*-axes. Thus, acetic acid can only permeate MOR membrane by penetrating the 12-ring throughout the membrane.

Based on the separation test results (Figs. 5 and 6), acetic acid permeation was not observed, indicating that very few 12-rings penetrated the membranes. Crystals inside a membrane layer would be randomly oriented regardless of the crystal orientation of the membrane surface, because the membrane orientations along the *c*-axis were formed by "evolutionary growth," as described above. Therefore, we deduced that acetic acid permeation was blocked at some grain boundaries where the two pathways (12- and 8-rings) collided. However, water was able to permeate such grain boundaries due to its small molecular size, resulting in both membranes showed the extremely high separation performance regardless of the orientation.

Another interesting feature is the permeation behavior of water. In the unary systems, the water flux through the *c*-oriented membrane was larger, possibly because water easily entered and diffused through the 12-ring. However, in the binary system, the water permeation through the *c*-oriented membrane was strongly hindered. In the *c*-oriented membrane, acetic acid easily entered the large pores and depressed the water flux. In contrast, it is difficult for acetic acid to enter micropores composed of the 8-ring, resulting in a randomly oriented membrane with relatively high water flux even in the binary system. The difference in crystal orientation on the surface affects the inhibition for water permeation by acetic acid in the binary mixture.

### *4.3. Adsorption Properties and Separation Principle*

As shown in Figs. 7 and 8, the amount of acetic acid adsorbed on the membrane in the unary system was approximately 30% less than that adsorbed on the powder. This result clearly showed that acetic acid cannot enter and diffuse across the entire membrane. In other words, a part of the 12-ring is not connected to the surface of the membrane.

Since the inner crystal layer of the membrane is composed of tiny particles with a random orientation, acetic acid may have to pass through 8-rings at least once to access the 12-rings inside the membrane. In contrast, there was little difference between the water adsorption properties of the powder and membrane, suggesting that water can diffuse and adsorb onto all the micropores in both the powder and membrane due to its small molecular size. Figure 9 shows a schematic diagram of the adsorption of water and acetic acid onto the powder and membrane. There may be a region through which water can and acetic acid cannot penetrate. This diagram can explain the extremely high separation performance of MOR membrane against the water/acetic acid mixture.

This phenomenon, in which relatively bulky molecules are unable to adsorb onto the crystals inside the membrane, has also been observed in other types of zeolite membranes. We have previously compared the adsorption properties of MFI-type zeolite powder and membrane [23,24]. The amount of *n*-hexane adsorbed onto the zeolite membranes was less than 65% of that adsorbed onto powder crystal, suggesting that there were portions where such molecules were inaccessible [23].

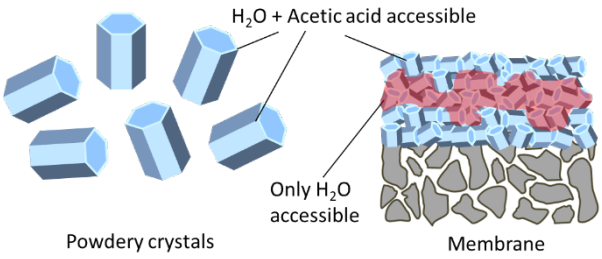


**Figure 9.** Schematic diagram of the adsorption of water and acetic acid on MOR powder and membrane.

### *4.4. Inhibition of Water Permeation by Acetic Acid*

We discuss the water permeation behavior in the binary system based on a typical surface diffusion model. In this model, the water flux through the zeolite membrane is dominated by two factors: the adsorbed amount and the diffusion rate [24,27,28]. In generally, adsorption is controlled by thermodynamics and permeation is determined by kinetics, and thus we should not confuse them. However, the adsorption phenomenon on the outer surface of a membrane during permeation tests often be according to a thermodynamic equilibrium. Therefore, we here discuss the permeation behavior on the basis of the results from adsorption tests and permeation tests.

In the binary systems, the water flux increased with increasing temperature and approached those in the unary systems. The behavior of water flux can be explained by the adsorbed amount of acetic acid, which inhibited water adsorption and diffusion in the micropores. The adsorbed amount of acetic acid tended to decrease at higher temperatures, in accordance with the thermodynamic equilibrium. Thus, the hindering effect of acetic acid weakened at higher temperatures.

The hindrance effect of the adsorbed acetic acid was quantitatively discussed based on the results of the adsorption tests in unary and binary systems on a membrane. The relative adsorbed amount of water, $A_R$ (−), was defined as shown in Equation (4);

$$A_R = A_B\, A_U^{-1} \tag{4}$$

where $A_B$ and $A_U$ represent the adsorbed amounts of water in the binary and unary systems, respectively. In addition, relative water flux, $J_R$, is expressed using $A_R$ and the relative diffusion rate, $D_R$ (−), in Equation (5), based on a typical surface diffusion model.

$$J_R = A_R\, D_R \tag{5}$$

$J_R$ and $A_R$ were calculated from the results of the permeation and adsorption tests shown in Figs. 6 and 7. Therefore, the effects of acetic acid inhibition on water adsorption and diffusion were independently evaluated. It is noted that we could not obtain the accurate values of the diffusion rates in both unary and binary systems, and $D_R$ just shows the ratio of the diffusion rate in unary to binary systems.

Table 1 lists $J_R$, $A_R$, and $D_R$ in the 50/50 kPa binary system at 398–543 K. Both of $A_R$ and $D_R$ were less than unity under all conditions, indicating that both water adsorption and diffusion in the micropores were disturbed by acetic acid. For example, the adsorbed amount and diffusion rate decreased by 19.8% and 20.8% at 398 K, respectively, resulting in the water flux in the binary system dropping to 63.5 % of that in the unary system. In addition, the inhibition by acetic acid weakened at high temperatures due to a decrease in the adsorbed amount of acetic acid; e.g., the water flux in binary system maintained 79.5% of that in unary system.

**Table 1.** $J_R$, $A_R$, and $D_R$ in the binary system of water/acetic acid (50/50 kPa).

| Temperature/K | Relative Water Flux $J_R$/- | Relative Adsorbed Amount $A_R$/- | Relative Diffusion Rate $D_R$/- |
|---|---|---|---|
| 398 | 0.635 | 0.802 | 0.792 |
| 473 | 0.695 | 0.871 | 0.798 |
| 543 | 0.795 | 0.882 | 0.901 |

## 5. Conclusions

The effect of crystal orientation and microstructure of the MOR zeolite membrane on the dehydration properties of a water/acetic acid mixture was studied. MOR membranes with different crystal orientations on the surface were prepared by varying the water content of the synthesis gel. Acetic acid hardly permeated through these MOR membranes, regardless of the crystal orientation, resulting in superior separation performance (a > 10,000).

The water flux through the MOR membrane in the binary systems is strongly influenced by the orientation of the crystals on the membrane surface. The water flux through the *c*-oriented membrane was significantly inhibited by the presence of acetic acid, suggesting that the acetic acid in the 12-rings along the *c*-axis hindered the adsorption and diffusion of water. In contrast, the randomly oriented membrane maintained a relatively high water flux in the presence of acetic acid because the acetic acid hardly entered the 8-rings along the *b*-axis.

Acetic acid inhibited water permeation via both adsorption and diffusion steps. The inhibition of water permeation became weaker at higher temperatures due to a decrease in the amount of adsorbed acetic acid.

## Author Contributions

M.S.: Conceptualization, Data curation, Investigation, Methodology, Writing of the original draft. M.N.: Data curation and Investigation. Y.I.: Data curation and Investigation. M.S.: Investigation, Methodology. M.M.: Conceptualization, Funding acquisition, Investigation, Resources, Supervision, Reviewing, and Editing. All authors have read and agreed to the published version of the manuscript.

## Funding

A part of this study was financially supported by Precise Measurement Technology Promotion Foundation and NEDO (Development of Fundamental Technologies for Green and Sustainable Chemical Processes).

## Data Availability Statement

The data will be made available on request.

## Conflicts of Interest

The authors declare no conflict of interest. The funders had no role in the design of the study; in the collection, analyses, or interpretation of data; in the writing of the manuscript; or in the decision to publish the results.

## References

1. Sholl, D.S.; Lively, R.P. Seven chemical separations to change the world. *Nature* **2016**, *532*, 435–437. https://doi.org/10.1038/532435a.
2. Yamaki, T.; Yoshimune, M.; Hara, N.; et al. Heat-integrated hybrid membrane separation-distillation process for energy-efficient isopropyl alcohol dehydration. *J. Chem. Eng. J.* **2018**, *51*, 890–897. https://doi.org/10.1252/jcej.18we039.
3. Amedi, H.R.; Aghajani, M. Economic Estimation of Various Membranes and Distillation for Propylene and Propane Separation. *Ind. Eng. Chem. Res.* **2018**, *57*, 4366–4376. https://doi.org/10.1021/acs.iecr.7b04169.
4. Zhang, Y.; Chen, S.; Shi, R.; et al. Pervaporation dehydration of acetic acid through hollow fiber supported DD3R zeolite membrane. *Sep. Purif. Technol.* **2018**, *204*, 234–242. https://doi.org/10.1016/j.seppur.2018.04.066.
5. Sun, W.; Wang, X.; Yang, J.; et al. Pervaporation separation of acetic acid–water mixtures through Sn-substituted ZSM-5 zeolite membranes. *J. Membr. Sci.* **2009**, *335*, 83–88. https://doi.org/10.1016/j.memsci.2009.02.037.
6. Hasegawa, Y.; Abe, C.; Ikeda, A. Pervaporative Dehydration of Organic Solvents Using High-Silica CHA-Type Zeolite Membrane. *Membranes* **2021**, *11*, 229. https://doi.org/10.3390/membranes11030229.
7. Nagase, T.; Kiyozumi, Y.; Hasegawa, Y.; et al. Dehydration of Concentrated Acetic Acid Solutions by Pervaporation Using Novel MER Zeolite Membranes. *Chem. Lett.* **2007**, *36*, 594–595. https://doi.org/10.1246/cl.2007.594.
8. Sato, K.; Sugimoto, K.; Kyotani, T.; et al. Synthesis, reproducibility, characterization, pervaporation and technical feasibility of preferentially *b*-oriented mordenite membranes for dehydration of acetic acid solution. *J. Membr. Sci.* **2011**, *385*, 20–29. https://doi.org/10.1016/j.memsci.2011.09.001.
9. Li, Y.; Zhu, M.; Hu, N.; et al. Scale-up of high performance mordenite membranes for dehydration of water-acetic acid mixtures. *J. Membr. Sci.* **2018**, *564*, 174–183. https://doi.org/10.1016/j.memsci.2018.07.024.
10. Matsukata, M.; Sawamura, K.; Shirai, T.; et al. Controlled growth for synthesizing a compact mordenite membrane. *J. Membr. Sci.* **2008**, *316*, 18–27. https://doi.org/10.1016/j.memsci.2007.11.037.
11. Li, G.; Kikuchi, E.; Matsukata, M. The control of phase and orientation in zeolite membranes by the secondary growth method. *Micropor. Mesopor. Mater.* **2003**, *62*, 211–220. https://doi.org/10.1016/S1387-1811(03)00407-4.
12. Lai, Z.; Bonilla, G.; Diaz, I.; et al. Microstructural Optimization of a Zeolite Membrane for Organic Vapor Separation. *Science* **2003**, *300*, 456–460. https://doi.org/10.1126/science.1082169.
13. Cao, T.; Pham, T.; Kim, H.S.; et al. Growth of Uniformly Oriented Silica MFI and BEA Zeolite Films on Substrates. *Science* **2011**, *334*, 1533–1538. https://doi.org/10.1126/science.1212472.
14. Kim, D.; Shete, M.; Tsapatsis, M. Large-Grain, Oriented, and Thin Zeolite MFI Films from Directly Synthesized Nanosheet Coatings. *Chem. Mater.* **2018**, *30*, 3545–3551. https://doi.org/10.1021/acs.chemmater.8b01346.

15. Sakai, M.; Kaneko, T.; Sasaki, Y.; et al. Formation Process of Columnar Grown (101)-Oriented Silicalite-1 Membrane and Its Separation Property for Xylene Isomer. *Crystals* **2020**, *10*, 949. https://doi.org/10.3390/cryst10100949.
16. Lu, X.; Wang, H.; Yang, Y.; et al. Microstructural manipulation of MFI-type zeolite films/membranes: Current status and perspectives. *J. Membr. Sci.* **2022**, *662*, 120931. https://doi.org/10.1016/j.memsci.2022.120931.
17. Banihashemi, F.; Lin, J.Y.S. *b*-Oriented MFI zeolite membranes for xylene isomer separation—Effect of xylene activity on separation performance. *J. Membr. Sci.* **2022**, *652*, 120492. https://doi.org/10.1016/j.memsci.2022.120492.
18. Wei, R.; Liu, X.; Zhou, Z.; et al. Carbon nanotube supported oriented metal organic framework membrane for effective ethylene/ethane separation. *Sci. Adv.* **2022**, *8*, eabm6741. https://doi.org/10.1126/sciadv.abm6741.
19. Sun, Y.; Hu, S.; Yan, J.; et al. Oriented ultrathin p-complexation MOF membrane for ethylene/ethane and flue gas separations. *Angew. Chem. Int. Ed.* **2023**, *62*, e202311336. https://doi.org/10.1002/anie.202311336.
20. Meier, W. The crystal structure of mordenite (clinoptilolite). *Cryst. Mater.* **1961**, *115*, 439–450. https://doi.org/10.1524/zkri.1961.115.16.439.
21. Santos, B.P.S.; Almeida, N.C.; Santos, I.S.; et al. Synthesis and Characterization of Mesoporous Mordenite Zeolite Using Soft Templates. *Cat. Lett.* **2018**, *148*, 1870–1878. https://doi.org/10.1007/s10562-018-2393-5.
22. Leeuwen, M.E. Derivation of Stockmayer potential parameters for polar fluids. *Fluid Ph. Equilib.* **1994**, *99*, 1–18. https://doi.org/10.1016/0378-3812(94)80018-9.
23. Sakai, M.; Sasaki, Y.; Kaneko, T.; et al. Contribution of Pore-Connectivity to Permeation Performance of Silicalite-1 Membrane; Part I, Pore Volume and Effective Pore Size. *Membranes* **2021**, *11*, 382. https://doi.org/10.3390/membranes11060382.
24. Sakai, M.; Sasaki, Y.; Kaneko, T.; et al. Contribution of Pore-Connectivity to Permeation Performance of Silicalite-1 Membrane; Part II, Diffusivity of $C_6$ Hydrocarbon in Micropore. *Membranes* **2021**, *11*, 399. https://doi.org/10.3390/membranes11060399.
25. Liu, Y.; Chen, S.; Ji, T.; et al. Room-Temperature Synthesis of Zeolite Membranes toward Optimized Microstructure and Enhanced Butane Isomer Separation Performance. *J. Am. Chem. Soc.* **2003**, *145*, 7718–7723. https://doi.org/10.1021/jacs.3c00009.
26. Mao, Y.; Zhou, Y.; Wen, H.; et al. Morphology-controlled synthesis of large mordenite crystals. *New J. Chem.* **2014**, *38*, 3295–3301. https://doi.org/10.1039/C3NJ01601C.
27. Bakker, W.J.W.; Van Den Broeke, L.J.P.; Kapteijn, F.; et al. Temperature Dependence of One-Component Permeation through a Silicalite-1 Membrane. *AIChE J.* **1997**, *43*, 2203–2214. https://doi.org/10.1002/aic.690430907.
28. Shindo, Y.; Hakuta, T.; Yoshitome, H.; et al. Gas Diffusion in Microporous Media in Knudsen's Regime. *J. Chem. Eng. J.* **1983**, *16*, 120–126. https://doi.org/10.1252/jcej.16.120.